Journal Pre-proofs

Multifunctional sodium alginate fabric based on reduced graphene oxide and polypyrrole for wearable closed-loop point-of-care application

Siyi Bi, Lei Hou, Yinxiang Lu

PII: S1385-8947(20)32906-5
DOI: https://doi.org/10.1016/j.cej.2020.126778
Reference: CEJ 126778

To appear in: *Chemical Engineering Journal*

Received Date: 22 May 2020
Revised Date: 19 August 2020
Accepted Date: 20 August 2020

Please cite this article as: S. Bi, L. Hou, Y. Lu, Multifunctional sodium alginate fabric based on reduced graphene oxide and polypyrrole for wearable closed-loop point-of-care application, *Chemical Engineering Journal* (2020), doi: https://doi.org/10.1016/j.cej.2020.126778

Multifunctional sodium alginate fabric based on reduced graphene oxide and polypyrrole for wearable closed-loop point-of-care application

Siyi Bi[a,b], Lei Hou[a], Yinxiang Lu[a,*]

[a]Department of Materials science, Fudan University, Shanghai 200433, China

[b]Andrew and Peggy Cherng Department of Medical Engineering, California Institute of Technology, Pasadena, CA 91125, USA.

Abstract

Sodium alginate (SA) fabrics decorated with reduced graphene oxide (rGO) and polypyrrole (PPy) serving as multifunctional materials are prepared by thermal-press reduction and in-situ polymerization. The superior conductivity (0.17 $k\Omega \cdot sq^{-1}$) of SA/rGO/PPy composite fabric is optimized through $L_9(3^4)$ orthogonal experimental design. Microstructures of the resultant SA/rGO/PPy composite fabric are investigated by field emission -scanning electron microscopy, Raman spectroscopy, X-ray photoelectron spectroscopy and X-ray diffraction measurement, respectively. It is found that SA/rGO/PPy composite fabric possesses not only excellent thermal stability but also mechanical durability. The results of NH_3 gas experiments indicate that SA/rGO/PPy composite fabric exhibits reliable linearity of concentration (2-16 ppm) dependency, unique repeatability, a high sensing response (10.7%) at low detection limit of 2 ppm and admirable selectivity. Moreover, SA/rGO/PPy composite fabric acting as a heater can reach to approximately 40-90 ℃ at low voltage of 3 V to 9 V. Hence, the optimum SA/rGO/PPy composite fabric is supposed to be used as ultrasensitive NH_3 gas sensor and wearable heater for nephropathy diagnosis purpose and thermo-responsive drug deliver in point-of-care (POC) application to develop a closed-loop treatment.

Keywords: flexible NH_3 gas sensing, wearable heater, thermal-press reduction, reduced graphene oxide, pyrrole in-situ polymerization

*Corresponding author. Tel. & fax: +86 21 55665059; E-mail address: yxlu@fudan.edu.cn

1. Introduction

The dramatically increase of aging population and life expectancy of human being force healthcare system to face increasing expenses and heavy burdens nowadays, which requires effective solutions to relieve pressure without elevating costs [1-2]. Smart wearable and implantable electronics such as actuators, sensors and wireless communication devices have been recently developed for point of care (POC) applications [3-5]. These devices can not only measure physiological and activity signals like heart rate, body temperature and blood pressure, but can also provide readouts for some specific pathologies like diabetes, renal illness and cardiovascular diseases [6-9]. Such approaches minimize the overall treatment expenditure and improve quality of life, leading to a fundamentally new path of healthcare management [10]. Recently, some researches indicate that the ammonia concentration in breath is associated with nephropathy, which is one of the most severe health issues in the world [11]. Due to the lose of dialysis function of kidneys for renal disease patients, urea will remain in blood and accumulate in form of ammonium ions which permeate through lung membrane via respiratory process as NH_3 gas at a level ranging from 0.82 ppm to 14.7 ppm (mean 4.88 ppm) in exhaled breath [12]. For the sake of diagnosis at early stage, several commercial detection techniques including biopsy, urine and blood tests are applied to evaluate indicators (blood urea nitrogen amount and glomerulus filtration rate) of nephropathy

[13]. However, these methods are invasive, and require expensive testing machines and additional skilled personnel in the hospital. Therefore, it is highly desirable to develop a non-invasive measurement for timely detection of renal disease while cost-effective and portable NH_3 gas sensor has become an ideal tool for disease diagnosis in POC system.

Currently, there are numerous studies on NH_3 gas sensors, mainly focus on exploiting sensing materials to improve sensitivity and selectivity [14]. The mainstream materials are metal oxides such as ZnO, TiO_2, SnO_2 and etc., which exhibit low detection limit but poor selectivity [15-16]. In addition, high operating temperature at 100 to 450 ℃ restrict their practical applications [17]. Graphene-based materials (namely graphene, GO and rGO) have been seen extensive usages in various gas sensors. Particularly, rGO with inherent characteristics including excellent stability, large theoretical specific surface area and structural defects on surface, is capable of offering increased binding sites for gas adsorption [18-20]. In addition, rGO are commonly obtained by means of reducing GO through reactive reductants like hydrazine, sodium borohydride and hydriodic acid [21]. These reductants are mostly toxic and may be harmful to human health and environment. Thermal reduction of GO has demonstrated as an effective and green method and the annealing temperature is as low as 200 ℃ [22]. Conductive polymers have shown enormous potential in volatile organic compounds (VOCs) detection at room temperature as a result of their unique sensitivity, short response time and easy processing [23-24]. Polypyrrole (PPy) in particular has been widely used due to its outstanding chemical stability, redox properties, surface charge tunable characteristics, ease of chemical synthesis and light weight [25-26]. Moreover, obvious improvement of pyrrole dispersion is observed due to the self-assembled pyrrole monomers on rGO surface via π−π stacking and electrostatic interaction, which means that the

combination of PPy and rGO are expected to have a synergistic effect on facilitating NH_3 sensing ability [27-28].

POC diagnostic systems with portable equipment and simple operations hold tremendous promise for early detection of disease at a curable stage [29]. Zeng *et. al.* developed a novel tactile chemomechanical biosensing platform for POC testing [30]. Yet the current POC managements always lack a real-time and effective treatment scheme against feedback of dynamic sensing so a closed-loop therapeutic system can be developed [31-32]. Targeted treatment triggered by sensing results can be achieved by drug deliver and different materials that are responsive to various stimuli involving electrical, light, thermal and magnetic as an alternative way to control drug release on demand have been studied [33-36]. Thermal-stimulated drug carriers considered as harmless materials will be locally released when temperature reaches the desired level, which can be achieved by a heater [37]. Thus, NH_3 sensing and thermal-sensitive drug delivering by heater in a closed-loop therapeutic system endows a significant possibility in POC management.

In this work, a layered rGO/PPy composite based on sodium alginate fabric (SA, a biocompatible cellulose-based textile) is fabricated by hot press method and in-situ polymerization, respectively. The optimized SA/rGO/PPy conductive composite is obtained by means of orthogonal experiment and acted as NH_3 gas sensor and thermal-sensitive drug deliver used heater in a closed-loop POC system. The NH_3 sensing performances of fabric composites are measured as a function of NH_3 concentration in natural environment containing nitrogen, oxygen, other rare gas and impurities. Further discussion in terms of gas sensing mechanism is thoroughly conducted. By applying different voltages to composites, the heating properties are investigated and can be tuned for drug delivery system.

Consequently, such layered SA/rGO/PPy composite fabrics with multifunction exhibit extraordinary prospects in wearable closed-loop POC application.

2. Experimental

2.1 Chemicals and Materials

The knitted sodium alginate fabric (SA, 240 g·cm^{-2}) in pure white were manufactured by Taicang Biqi Novel Material Co. Ltd. Graphene oxide (GO) was initially prepared from graphite flakes by a typical Hummers method. Polyvinylpyrrolidone (PVP), pyrrole (Py) monomer, ferric chloride hexahydrate ($FeCl_3 \cdot 6H_2O$) and sodium anthraquinone-2-sulfonate (SAQS) were purchased from Sigma-Aldrich. All other chemicals were of analytical grade and were used without further purification unless otherwise mentioned. Deionized (DI) water (18.2 MΩ cm) was used in whole experiments for solutions, synthesis and rinsing.

2.2 Thermal-press reduction of GO

SA fabric was pre-cleaned with acetone and non-ionic detergent to remove impurities and grease, following rinsing with DI water and drying. To obtain a well-dispersed GO solution, a certain amount of GO powder was sonicated in 200 ml DI water with 100 mg PVP as dispersant for 30 min. SA fabric was then immersed in GO aqueous solution with magnetic stirring for 30 min for thoroughly adsorption and GO-deposited SA fabric (SA/GO) was dried in an oven at 80 ℃ for 30 min. The SA/GO fabric was hot pressed with a flat heat machine (PTJ38, Yiwu Maike Digital Imaging Co., Ltd, China) at certain temperature for a period time to reduce GO to reduced GO (rGO). In order to have an optimal thermal-press condition, an orthogonal experimental design was applied by using Orthogonal Design Assistant II software (Sharetop Software Studio). Variables including GO concentration (1, 3 and 5 mg·ml^{-1}),

thermal-press temperature (160, 180 and 200 ℃) and time (30, 60 and 90 min) were identified to have significant effects on conductivity of rGO coated SA fabric (SA/rGO). Therefore, a $L_9(3^4)$ matrix which is an orthogonal array of three factors and three levels was employed to assign the considered factors and levels as displayed in Table S1.

2.3 In-situ polymerization of Py monomer

The optimal SA/rGO fabric was then used as the backbone for Py polymerization. In a typical in-situ chemical synthesis process, Py monomer along with the same concentration of dopant (SAQS) was added to 200 ml DI water and sonicated in ice bath until no obvious aggregations were observed. The SA/rGO fabric was then soaked in as-prepared Py monomer solution for 30 min at 4 ℃ so that Py monomer can penetrate into the fabric. Oxidant solution was prepared by dissolving $FeCl_3 \cdot 6H_2O$ in 200 ml DI water under magnetic stirring for 10 min at room temperature. The in-situ polymerization reaction was performed by titrating oxidant solution into Py monomer solution in ice bath and the color of the solution changed almost instantaneously to black once the reaction was occurred. After polymerization, the PPy deposited fabric (SA/rGO/PPy) was sequentially rinsed with DI water to remove unreacted Py monomer and blank PPy powders, and dried in an oven for 30 min at 60 ℃. Orthogonal $L_9(3^4)$ experimental design was used in PPy synthesis as well to obtain an optimized SA/rGO/PPy fabric. The concentration of Py monomer solution (0.1, 0.2 and 0.3 $mol \cdot L^{-1}$), ratio of Py monomer and oxidant (2:1, 1:1 and 1:2) and reaction time (60, 120 and 180 min) were designed as factors and levels in Table S2. In addition, PPy coated SA fabric (SA/PPy) was also prepared as a control group. The whole fabrication process of optimal SA/rGO/PPy fabric was illustrated in Fig. 1.

2.4 Characterization of microstructures and durable performance

The fabric samples were conditioned at 20 ± 2°C and 65 ± 2% relative humidity for 24 h prior to measurements. Morphologies of fabric samples were observed by a field emission-scanning electron microscope (FE-SEM, S-4300SE, Hitachi, Japan). Laser Raman spectrometer (inVia, Renishaw, Britain) operating a laser at wavelength of 514 nm and power of 25 mW was utilized to perform Raman spectra investigations in the range of 500 to 3000 cm^{-1}. X-ray photoelectron spectroscopy (XPS) spectra were carried out on an X-ray photoelectron spectrometer (Thermo ESCALAB 250XI) using aluminum Kα x-ray beam as the excitation source. Crystallographic information for the fabric samples were studied using an X-ray diffraction (XRD, Rigaku D/MAX-2500, Japan) with Cu Kα radiation. Surface resistances (R_s) of the fabric samples were recorded by a digital four-point probe (ST2258C, China) and at least five measurements were conducted to obtain average values. Tensile strength of the fabric samples was performed on an electronic fabric strength tester (CMT-4304-QY) according to GB/ T 3923.1-1997 standard. Thermogravimetric analyzer (TGA, DTG-60H, SHIMADZU, Japan) was employed to investigate the thermal stability for fabric samples in nitrogen atmosphere with heating rate of 5 °C/min from 30 °C to 1000 °C. The fabric samples were subjected to various numbers of domestic washing and drying procedures based on GB/T 17595-1998 for water durability test. Electrical performances were compared before and after 3, 6, 9 and 12 laundry cycles to validate the serviceability of fabric samples.

2.5 Characterization of sensing and heating behaviors

The NH_3 gas sensing characteristics of fabric samples were analyzed on a homemade gas handling system. Basically, the SA/rGO/PPy fabric was mounted in a closed chamber and well-coated with silver paste (Ausbond®) at two ends for electrical connection. The change in electrical resistance was measured by LCR meter (IM 3590, HIOKI, Japan) at various NH_3

gas concentration (2-16 ppm). Desired NH_3 gas concentration was well-controlled by diluting 100 ppm NH_3 with wet air. The sensing measurement was conducted at practical environment as atmospheric pressure, room temperature and wet air (50% relative humidity). The sensing response of SA/rGO/PPy fabric was defined as the equation (1):

$$R_{rel}\ (\%) = (R_{NH3}\text{-}R_0)/R_0 \times 100\% \quad (1)$$

where R_0 was the base value of electrical resistance and R_{NH3} was the variational electrical resistance upon exposure to NH_3 gas. To investigate the heating performance, a constant voltage (3-9 V) provided by DC power supply (RXN-30) was applied to SA/rGO/PPy fabric with an area of 2 cm × 2 cm. Meanwhile, a thermometer (UT320V3.01) was utilized to record the real-time temperature on the surface of SA/rGO/PPy fabric.

3. Results and discussion

3.1 Optimization of preparation conditions

Since various parameters potentially affect the process of GO thermal-press reduction and Py monomer in-situ polymerization, the optimization of experimental conditions is a critical step for the improvement of green and efficient fabrication method. Parameters including GO concentration, thermal-press temperature and time for thermal-press reduction of GO are optimized while concentration of Py monomer solution, ratio of Py monomer and oxidant and reaction time are taken into consideration for in-situ polymerization of Py monomer. In both optimization experiments, average R_s values and standard deviation (SD) are used for the evaluation indices of the preparation of SA/rGO/PPy fabric. The results of experiments, calculated K values (average of the same level) and R values (K values range) are displayed in Table 1 and Table 2, respectively. Optimal level of factors for fabrication process is

achieved by comparing different K values meanwhile R values reflect the most significant determinant of the level on average R_s and its SD. It is observed in Table 1 that the thermal-press temperature plays an important role in R_s value and SD for GO reduction followed by thermal-press time and GO concentration. The optimal parameters for SA/rGO fabric to obtain a lowest R_s value (3.14 $k\Omega \cdot sq^{-1}$) are that GO concentration of 5 $mg \cdot ml^{-1}$, reaction temperature at 200 ℃ and reaction time of 60 min. Optimization experiment of Py monomer polymerization is then conducted on the basis of superior SA/rGO fabric. The results in Table 2 show that the influences on conductivity decreases in the order: ratio of Py monomer and oxidant > concentration of Py monomer solution > reaction time. The optimum preparation conditions for SA/rGO/PPy fabric (lowest R_s value of 0.17 $k\Omega \cdot sq^{-1}$) based on orthogonal experimental design are the ratio of 1:2, Py concentration of 0.3 $mol \cdot L^{-1}$ and reaction time of 120 min.

3.2 Morphologies and microstructures of SA/rGO/PPy fabric

Fig. 2 successively presents the morphologies of SA fabric, SA/GO fabric, SA/rGO fabric and SA/rGO/PPy composite fabric. The pristine SA fabric in Fig. S1 and Fig. 2a shows a typically fibrous structure with fibers twisting with each other and a relatively smooth surface with little impurities but some trenches owing to the wet-spinning process of SA fibers. After SA fabric is deposited with GO, flake layers are observed visibly to be affixed to the surface of SA fibers from SEM image in Fig. 2b, which indicates the successful assembly of GO sheets on fabrics. Morphologies of different GO concentrations on fabrics are characterized in Fig. S1 and the roughness of surface becomes more significant with the increased GO concentration. Grooves, wrinkled and rippled structures of rGO nanosheets verify the reduction of GO on SA fabric surface during thermal-press procedure as shown in Fig. 2c. In

addition, smooth fiber surface and gaps between SA fibers are disappeared and completely covered by rGO nanosheets. Fig. 2d demonstrates that PPy nanoparticles with cauliflower-like structure are homogeneously distributed on the surface of rGO nanosheets. Py monomers containing a number of sp2 carbon atoms are firstly adsorbed on the surface of rGO attributed to electrostatic attraction and polymerized in the presence of $FeCl_3$. A closer observation of PPy layer in the inserted image in Fig. 2d indicates that PPy nanoparticles have a spherical granular structure with particle size in the range of 200 to 500 nm. Such porous morphology of SA/rGO/PPy composite fabric is advantageous to the adsorption of NH_3 gas molecules, resulting in superior sensitivity.

Raman spectrum (in the range of 500 to 3000 cm^{-1}) reflecting structural changes during thermal-pressing and in-situ polymerization to form SA/rGO/PPy composite fabric are shown in Fig. 3a. The fundamental bands of pristine SA fabric (regenerated cellulose) are observed and the characteristic signals of cellulose are presented at 1090 cm^{-1} and 1106 cm^{-1}, which are associated with asymmetric stretching vibration of C-O-C glycosidic linkage. Bands revealed at 1294 cm^{-1} and 1380 cm^{-1} are assigned to C-OH bonds and symmetric vibration of C-H bond, respectively. Additionally, signals observed at 682 cm^{-1}, 789 cm^{-1}, 891 cm^{-1} and 994 cm^{-1} can be ascribing to C-OH, O-H, C-H and C-O bonds, respectively. To verify GO thermal-press reduction, Raman spectrum of SA/GO fabric and SA/rGO fabric are displayed in Fig. 3a. Two prominent peaks at 1343 cm^{-1} and 1589 cm^{-1} corresponding to D peak (disordered sp3 C atoms) and G peak (ordered sp2 C atoms) of graphitic materials are identified in SA/GO fabric. However, the D band and G band peak shift to 1340 cm^{-1} and 1584 cm^{-1}, respectively for SA/rGO fabric and the intensity ratio of D and G band (ID/IG=1.12) of SA/rGO fabric is higher compared to that of SA/GO fabric (ID/IG=0.95).

This is an indicator of the shrinkage in size of graphitic domains and sp2 cluster number during thermal-press reduction, which further discloses the high reduction efficiency of heating condition. Two typical peaks of SA/PPy fabric at 1048 cm^{-1} and 1566 cm^{-1} (Fig. 3a) are attributable to C=C stretching vibration and C-H in-plane deformation vibration in PPy. Moreover, peaks at 962 cm^{-1} and 1336 cm^{-1} are attributed to the ring-stretching mode of PPy in SA/PPy fabric. For Raman analysis of SA/rGO/PPy composite fabric, peaks belonging to rGO layer and PPy layer (at 961 cm^{-1}, 1047 cm^{-1}, 1348 cm^{-1} and 1569 cm^{-1}, respectively) are detected while those contributed to SA substrate are disappeared, confirming the uniform and compact coverage of rGO and PPy on SA fabric.

XPS is employed to investigate the quantitative elemental compositions and chemical states of SA/GO fabric, SA/rGO fabric, and SA/rGO/PPy fabric as shown in Fig. S2 and Fig. 3(b-e). The main elements of C, N and O are obviously seen in XPS survey spectra in Fig. S2. The C1s spectra of SA/GO fabric in Fig. 3b can be deconvoluted into four peaks at binding energy of 284.7 eV (C-C/C=C), 286.5 eV (C-O), 287.1 eV (C=O) and 288.3 eV (O=C-O). Compared with SA/GO fabric, the intensity of three C-O bonding peaks in SA/rGO fabric (Fig. 3c) decrease significantly implying the success of GO reduction. Moreover, the C/O atomic ratio (1.20) of SA/GO fabric is lower than that of SA/rGO fabric (6.82) due to the reducing amount of residual oxygenated groups after thermal-press treatment, which is consistent with Raman results. The decomposed Gaussian peaks of C1s for SA/rGO/PPy fabric (in Fig. 3d) are located at binding energy at 283.3 eV, 284.5 eV and 286.1 eV corresponding to C-C, C-N and C-O, respectively. N1s XPS core-level spectra for SA/rGO/PPy fabric (shown in Fig. 3e) is deconvoluted into two Gaussian peaks with binding energy of 399.28 eV (C-N/N-H) and 400.5 eV (C-N=O) confirming the presence of PPy.

XRD pattern of SA/rGO/PPy composite fabric is displayed in Fig. 3f and the crystalline identities of fabric samples in each step are shown in Fig. S3. The peak at 2θ = 10.7° (with d-spacing of 0.83 nm) corresponds to (0 0 1) of GO in SA/GO fabric while a broad diffraction peak at 2θ = 28.0° (with d-spacing of 0.32 nm) and a weak peak at 2θ = 41.5° are observed in the XRD pattern of SA/rGO fabric (Fig. S3). The reduction in d-spacing verifies the removal of oxygen trapped between GO nanosheets during thermal-press reduction. For SA/rGO/PPy composite fabric, a small intense peak appeared at 2θ = 41.5° and broad peak located at 2θ = 28.4°are characteristic diffraction peaks for graphite like structure of rGO and amorphous structure of PPy, respectively. The overlapping diffraction peaks of rGO and PPy indicate the formation of SA/rGO/PPy composite fabric during in-situ synthesis process.

3.2 Durability of SA/rGO/PPy composite fabric

Durability is essential to the practical application of SA/rGO/PPy composite fabric, hence, measurements including tensile strength, thermal stability and fastness to washing are carried out as shown in Fig. 4. Typical stress-strain curve of SA/rGO/PPy composite fabric (wale direction) during stretching is plotted in Fig. 4a and it exhibits high breaking strength (95.48 MPa) and elongation rate (139.35%) due to the knitted structure of SA substrate, which also implies that high temperature during thermal-pressing do not cause damage on fabrics. The relationship between temperature and weight change is illustrated by thermogravimetric analysis as shown in Fig. 4b. In TGA curve of SA/rGO/PPy composite fabric, dramatic mass loss of 59.01% in the temperature range of 100 °C to 800 °C is caused by dehydration of SA substrate, decomposition of functional groups in rGO and PPy components. Fastness to washing is tested to estimate the bonding strength of decorated rGO/PPy nanosheets with SA fabric. Surface resistances of SA/rGO/PPy composite fabric before and after repeated washing

cycles are recorded in Fig. 4c. It can be seen that the conductivities of SA/rGO/PPy composite fabrics suffering from three laundry procedures increase slightly compared to that of original fabric without washing (from 174 ± 5 $\Omega \cdot sq^{-1}$ to 181 ± 6 $\Omega \cdot sq^{-1}$). It is noteworthy that the resistance of SA/rGO/PPy composite fabrics (211 ± 6 $\Omega \cdot sq^{-1}$) has little variations even after 12 cycles of laundry due to the hydrophobic nature of PPy, which reveals an admirable waterproof ability.

3.3 NH_3 sensing behaviors of SA/rGO/PPy composite fabric

The explorations of SA/rGO/PPy composite fabrics as sufficient materials for NH_3 sensing performance is conducted by recording R_{rel} of fabric samples exposing to NH_3 gas. The real-time dynamic response towards different NH_3 gas concentrations within the range of 2-16 ppm at room temperature is plotted in Fig. S4 and Fig. 5a. The response of SA/rGO/PPy composite fabric undergoes an abruptly upward tendency in the initial few seconds and then gradually approaches steady level upon exposure to target gas concentration. The response time refers to the time reaching 90% of total electrical resistance variation whereas recovery time is defined as the time required to recovering to 90% of the initially measured electrical resistance. The SA/rGO/PPy sensor exhibits a 90% response time of about 19 s and a 90% recovery time of about 24 s toward 16 ppm NH_3 exposure. Sensing response of SA/rGO/PPy composite fabric is increased with the increment of NH_3 gas concentration. The power-law of dependence between response and NH_3 concentration can be found in SA/rGO/PPy composite fabric because gas adsorption is not uniform across heterogeneous surfaces. Based on Freundlich adsorption isotherm, concentration dependency obeys the following equation (2):

$$\frac{\triangle R}{R_0} \propto \frac{\alpha C^{\beta}}{1 + \alpha C^{\beta}} \quad (2)$$

where $\triangle$R, C, α and β denote the resistance variation before and after NH_3 gas adsorption,

NH_3 gas concentration, a proportionality factor, and the exponent. Since the concentration of NH_3 gas is relatively low, the equation can be simplified as: $\frac{\triangle R}{R_0} \propto \alpha C^{\beta}$. The relationship between logarithmic sensing response and logarithmic NH_3 concentration suggests a commendable linearity with a slope of 0.8469 and R square of 0.9784 as depicted in Fig. 5b. To identify the lowest detection of NH_3 gas concentration, SA/rGO/PPy composite fabric is subjected to 1 ppm NH_3 gas (Fig. S5). The result indicates that no discernible variations in resistances are obtained, which means the limits of detection is taken to be 2 ppm. Moreover, the sensing response and sensitivity at minimal detection limit (2 ppm) is about 10.7% and 5.4%/ppm, respectively, which is superior to those of NH_3 sensors in the literature listed in Table 3.

SA/rGO/PPy composite fabric with ultrahigh sensitivity then experiences 5 and 100 successive cycles of NH_3 gas exposure at 3 ppm (in Fig. 5c and Fig. S6), respectively, demonstrating a repeatable response of 12.4 ± 0.46%. The excellent reproducibility of SA/rGO/PPy composite fabric is evaluated by testing five batch samples at different NH_3 gas concentration as revealed in Fig. S7. Sensing responses of SA/rGO/PPy composite fabric are also relatively stable for a long period time observation (Fig. S8), which implies the reliable serviceability as a NH_3 gas sensor. Furthermore, SA/rGO/PPy fabric displays an ignorable response to humidity (compared with NH_3 gas sensing) when RH is lower than 85%, and specifically, less than 3% variation in R_{rel} value with a change of 10% RH when RH is higher than 85% (Fig. S9). No obvious variations are observed for NH_3 sensing performance after 500 times bending tests (radii of curvature is 1 mm) as demonstrated in Fig. S10, which indicates that SA/rGO/PPy fabric is flexible enough for wearable sensing applications.

The selectivity of SA/rGO/PPy sensor is demonstrated in Fig. 5d, in comparison with other

analytes involving ethanol, methanol, acetone, toluene, hexane, chloroform, H_2, CO, CO_2, SO_2 and NO_2. The saturated concentrations of vapors are generated at room temperature by diluting with dry air to 1%. The concentrations of gaseous detection (H_2, CO, CO_2, SO_2 and NO_2) are fixed at 500 ppm, except that of NH_3 gas (5 ppm). The results suggest that SA/rGO/PPy sensor exhibits predominant selectivity to NH_3 gas even the concentration of interfering gases are 100 times higher than that of NH_3 gas. It is noteworthy that when SA/rGO/PPy sensor is exposed to CO_2 and NO_2, negative responses are observed as shown in Fig. 5d. This phenomenon is explained by accepting electrons from SA/rGO/PPy composite fabric by strong oxidizing gas (i.e. CO_2 and NO_2), leading to the increase of hole density and decrease of electrical resistance. Therefore, in the case of simultaneous presence of CO_2, NO_2 and NH_3 gas, the sensing response of SA/rGO/PPy composite fabric will decline owing to the complementarity or competition between electron acceptors (CO_2 and NO_2) and electron donors (NH_3). To our best knowledge, the concentration of CO_2 in the exhaled air is higher than normal air, however, little influence will be generated on the overall response, which reveals a great potential for NH_3 gas detection in breathing.

The sensing behavior of SA/rGO/PPy composite fabric is in accordance with sensing characteristics of p-type semiconductor, exhibiting the increase of resistance when exposed to NH_3 gas. The possible mechanism is proposed to be a deprotonation/protonation process through NH_3 gas adsorption/desorption on the surface of composite fabric (in Fig. 1). When electron-donating NH_3 molecules adsorb onto PPy surface, the doublet of nitrogen in NH_3 loses an electron to the nitrogen of π backbone of PPy through electrons transfer, which acts as a dedoping (deprotonation) process, giving rise to the increase of resistance in PPy. After NH_3 gas removal, the electrons in backbone of PPy are back to NH_3 and the neutralized PPy

recovers the resistance to the initial value. The deprotonation/protonation process is followed by the equation (3) and equation (4).

$PPy^{+} + NH_3 \rightarrow PPy^{0} + NH_3^{+}$ Adsorption (3)

$PPy^{0} + NH_3^{+} \rightarrow PPy^{+} + NH_3$ Desorption (4)

The resistance changing in electron transfer occurred on the surface of PPy can be effectively transferred to rGO due to the good interfacial affinity. rGO with high density of sp2-bonded carbon, vacancies, structural defects and residual oxygen functional groups builds a hole-transporting matrix, function as a p-type semiconductor. The electrons transfer depletes holes in the matrix and thus increase the resistance of rGO. The synergistic effect of PPy and rGO enhances the sensing response of SA/rGO/PPy composite fabric to NH_3 gas by facilitating electrons transfer between NH_3 molecules and composite fabric. In addition, a gas-sensing model (detailed in Supplementary material) is established for SA/rGO/PPy composite fabric and expressed as:

$$\triangle R = (r_1 - r_0)\frac{m}{n}\frac{K_m C_0}{1 + K_m C_0} \quad (5)$$

where r_0, r_1, K_m and C_0 are resistance of vacant site, resistance of occupied site, constant of adsorption equilibrium and concentration of gas. The overall resistance of SA/rGO/PPy composite fabric is considered as n resistance of R in parallel and each R is composed of m resistance of r in series. R and r present the resistance of sensing layer and site while n and m denote the number of conduction paths and active sites, respectively. As a result, a thinner sensing material with lower n value (less conduction paths) and higher m value (more active sites) will generate a better sensing response signal. The SA/rGO fabric prepared by thermal-press reduction discloses a relatively smooth surface as shown in Fig. S11 because of the

pressure during pressing, meanwhile reduce the thickness of sensing layer compared with other fabrication methods (like CVD and using reductants). In addition, PPy deposited on rGO surface will boost the active sites (i.e. promote m value). Therefore, SA/rGO/PPy composite fabric with relatively smooth rGO surface (lower n value) and PPy activated sites (higher m value) possesses an extraordinary sensing response.

3. 4 Joule heating performance of SA/rGO/PPy composite fabric

In drug delivering system, heater is a significant module to trigger the release of thermal-responsive drug carriers. The heating performance of SA/rGO/PPy composite fabric is evaluated by monitoring the temperature of central region on composite fabric with an electronic thermometer. The variations in temperature versus time at different applied voltages are plotted in Fig. 6a. When voltage is applied to the conductive fabric, temperature increases rapidly and reaches a relatively high and stable stage, while it decreases slowly to the initial value after removing voltage. The maximum temperature increases with the increment of voltage and the maximum surface temperature ranges from 42.4 ℃ to 88.9 ℃ within the voltage of 3-9 V. It is noteworthy that the optimum operating temperature of heater is approximately 40 ℃ - 45 ℃ and the safe voltage for human being is below 24V. Thus, this portable SA/rGO/PPy composite fabric as heater is capable of generating suitable temperature by commercial battery. The relationship between measured temperature and applied voltage is determined by Joule's law and the results (in Fig. 6b) manifest an excellent linear correlation with R square of 0.9918. In order to prove the durability of SA/rGO/PPy composite fabric, the bending influence on heating performance is examined. SA/rGO/PPy composite fabric is suffered from various bending times and the temperature (at 3 V) retains stable even after 1000 times bending (in Fig. S12). The results indicate that SA/rGO/PPy composite fabric with

outstanding heating property is admirable for practical usage in closed-loop drug delivering system.

Conclusions

Wearable SA/rGO/PPy composite fabric is obtained through an environmental-friendly thermal-press method and simple in-situ polymerization. SA/rGO/PPy composite fabric with superior conductivity (Rs value of 0.17 $k\Omega \cdot sq^{-1}$) is optimized through $L_9(3^4)$ orthogonal experimental design. The optimal parameters for GO reduction are GO concentration of 5 $mg \cdot ml^{-1}$, reaction temperature at 200 ℃ and reaction time of 60 min while for Py monomer polymerization are the ratio (Py monomer and oxidant) of 1:2, Py concentration of 0.3 $mol \cdot L^{-1}$ and reaction time of 120 min. The optimum SA/rGO/PPy composite fabric is able to detect NH_3 gas at low concentration (2-16 ppm) and exhibits an extraordinary sensing response of 10.7% at minimal detection limit of 2 ppm due to the synergistic effect of PPy and rGO. It is notable that the selectivity of SA/rGO/PPy composite fabric among volatile organic compounds and gases is admirable as well. In addition, SA/rGO/PPy composite fabric can be heated to above 40 ℃ at applied voltage of 3 V, which demonstrates a function as heater. Such versatility grant SA/rGO/PPy composite fabric ideal opportunity to act as ultrasensitive NH_3 gas sensor and wearable heater for renal disease diagnosis (which requires a typical NH_3 gas detection range of 2 ppm to 15 ppm) and effective drug deliver in closed-loop POC treatment.

Conflicts of interest

Declarations of interest: none

Acknowledges

This work was supported by the National Natural Science Foundation of China (No. U1830108), the Innovation Foundation of Shanghai Aerospace Science and Technology (No. SAST2018-061), the program of China Scholarships Council (No. 201906100112).

References

[1] H.Z. Huang, S. Su, N. Wu, H. Wan, S. Wan, H.C. Bi, L.T. Sun, Graphene-based sensors for human health monitoring, Front. Chem. 7 (2019) 399.

[2] J. Kim, A.S. Campbell, B.E. Avila, J. Wang, Wearable biosensors for healthcare monitoring, Nat. Biotechnol. 37 (2019) 389-406.

[3] J. Shu, Z.L. Qiu, Q. Zhou, D.P. Tang, A chemiresistive thin-film translating biological recognition into electrical signals: an innovative signaling mode for contactless biosensing, Chem. Commun. 55 (2019) 3262-3265.

[4] Z.Z. Yu, Y. Tang, G.N. Cai, R.R. Ren, D.P, Tang, Paper electrode-based flexible pressure sensor for point-of-care immunoassay with digital multimeter, Anal. Chem. 91 (2018) 1222-1226.

[5] J.F. Gao, B. Li, X.W. Huang, L. Wang, L.W. Lin, H. Wang, H.G. Xue, Electrically conductive and fluorine free superhydrophobic strain sensors based on SiO_2/graphene-decorated electrospun nanofibers for human motion monitoring, Chem. Eng. J. 373 (2019) 298-306.

[6] Y.X. Li, T.Y. He, L.J. Shi, R.R. Wang, J. Sun, Strain sensor with both a wide sensing

range and high sensitivity based on braided graphene belts, ACS Appl. Mater. Inter. 12 (2020) 17691-17698.

[7] Y. Zhai, Y.F. Yu, K.K. Zhou, Z.G. Yun, W.J. Huang, H. Liu, Q.J. Xia, K. Dai, G.Q. Zheng, C.T. Liu, C.Y. Shen, Flexible and wearable carbon black/thermoplastic polyurethane foam with a pinnate-veined aligned porous structure for multifunctional piezoresistive sensors, Chem. Eng. J. 382 (2020) 122985.

[8] Y. Yang, Y. Song, X.J. Bo, J.H. Min, O.S. Pak, L.L. Zhu, M.Q. Wang, J.B. Tu, A. Kogan, H.X. Zhang, T.K. Hsiai, Z.P. Li, W. Gao, A laser-engraved wearable sensor for sensitive detection of uric acid and tyrosine in sweat, Nat. Biotechnol. 38 (2020) 2017-224.

[9] Y.J. Hong, H. Jeong, K.W. Cho, N.S. Lu, Wearable and implantable devices for cardiovascular healthcare: from monitoring to therapy based on flexible and stretchable electronics, Adv. Funct. Mater. 29 (2019) 1808247.

[10] Y. Yang, W. Gao, Wearable and flexible electronics for continuous molecular monitoring, Chem. Soc. Rev. 48 (2019) 1465-1491.

[11] T.N. Ly, S. Park, Highly sensitive ammonia sensor for diagnostic purpose using reduced graphene oxide and conductive polymer, Sci. Rep. 8 (2018) 1-12.

[12] T.W. Sung, Y.L. Lo, Ammonia vapor sensor based on CdSe/SiO_2 core–shell nanoparticles embedded in sol–gel matrix, Sensor Actuat. B-Chem. 188 (2013) 702-708.

[13] T. Shafi, W.M. Michels, A.S. Levey, L.A. Inker, F.W. Dekker, R.T. Krediet, T. Hoekstra, G.J. Schwartz, J.H. Eckfeldt, J. Coresh, Estimating residual kidney function in dialysis patients without urine collection, Kidney. Int. 89 (2016) 1099-1110.

[14] Y.F. Huang, W.C. Jiao, Z.M. Chu, S.Y. Wang, L.Y. Chen, X.M. Nie, R.G. Wang, X.D. He, High sensitivity, humidity-independent, flexible NO_2 and NH_3 gas sensors based on SnS_2

hybrid functional graphene ink, ACS Appl. Mater. Inter. 12 (2019) 997-1004.

[15] P. Tiwary, N. Chakrabarty, A.K. Chakraborty, R. Mahapatra, Flower-like ZnO nanostructures as gas sensor, Mater. Today, 11 (2019) 875-878.

[16] A.M. Al-Enizi, M. Naushad, A.H. Al-Muhtaseb, Ruksana, S.M. Alshehri, Z.A. Alothman, T. Ahamad, Synthesis and characterization of highly selective and sensitive Sn/SnO_2/N-doped carbon nanocomposite (Sn/SnO_2@ NGC) for sensing toxic NH_3 gas, Chem. Eng. J. 345 (2018) 58-66.

[17] W. Wei, W. Li, L.L. Wang, High-selective sensitive NH_3 gas sensor: A density functional theory study, Sensor Actuat. B-Chem. 263 (2018) 502-507.

[18] R.J. Zeng, Z.B. Luo, L.J. Zhang, D.P. Tang, Platinum nanozyme-catalyzed gas generation for pressure-based bioassay using polyaniline nanowires-functionalized graphene oxide framework, Anal. Chem. 90 (2018) 12299-12306.

[19] L.S.K. Achary, A. Kumar, B. Barik, P.S. Nayak, N. Tripathy, J.P. Kar, P. Dash, Reduced graphene oxide-$CuFe_2O_4$ nanocomposite: A highly sensitive room temperature NH_3 gas sensor, Sensor Actuat. B-Chem. 272 (2018) 100-109.

[20] C.T. Lee, Y.S. Wang, High-performance room temperature NH_3 gas sensors based on polyaniline-reduced graphene oxide nanocomposite sensitive membrane, J. Alloy. Compd. 789 (2019) 693-696.

[21] L.G. Guex, B. Sacchi, K.F. Peuvot, R.L. Andersson, A.M. Pourrahimi, V. Strom, S. Farris, R.T. Olsson, Experimental review: chemical reduction of graphene oxide (GO) to reduced graphene oxide (rGO) by aqueous chemistry, Nanoscale, 9 (2017) 9562-9571.

[22] J.S. Rem, C.X. Wang, X. Zhang, T. Carey, K.L. Chen, Y.J. Yin, F. Torrisi, Environmentally-friendly conductive cotton fabric as flexible strain sensor based on hot press

reduced graphene oxide, Carbon, 111 (2017) 622-630.

[23] N. Indarit, Y.H. Kim, N. Petchsang, R. Jaisutti, Highly sensitive polyaniline-coated fiber gas sensors for real-time monitoring of ammonia gas, Rsc Adv. 9 (2019) 26773-26779.

[24] C.B. Lim, J.B. Yu, D.Y. Kim, H.G. Byun, D.D. Lee, J.S. Huh, Sensing characteristics of nano-network structure of polypyrrole for volatile organic compounds (VOCs) gases, Sensor, (2006) 695-698.

[25] Y.X. Qin, Z. Cui, T.Y. Zhang, D. Liu, Polypyrrole shell (nanoparticles)-functionalized silicon nanowires array with enhanced NH_3-sensing response, Sensor Actuat. B-Chem. 258 (2018) 246-254.

[26] J. Shu, Z.L. Qiu, S.Z. Lv, K.Y. Zhang, D.P. Tang, Cu^{2+}-doped SnO_2 nanograin/polypyrrole nanospheres with synergic enhanced properties for ultrasensitive room-temperature H_2S gas sensing, Anal. Chem. 89 (2017): 11135-11142.

[27] X.H. Tang, J.P. Raskin, N. Kryvutsa, S. Hermans, O. Slobodian, A.N. Nazarov, Marc. Debliquy, An ammonia sensor composed of polypyrrole synthesized on reduced graphene oxide by electropolymerization, Sensor Actuat. B-Chem. 305 (2020) 127423.

[28] J. Shu, Z.L. Qiu, D.P. Tang, Self-referenced smartphone imaging for visual screening of H_2S using Cu_xO-polypyrrole conductive aerogel doped with graphene oxide framework, Anal. Chem. 90 (2018) 9691-9694.

[29] Z.Z. Yu, G.N. Cai, P. Tong, D.P. Tang, Saw-toothed microstructure-based flexible pressure sensor as the signal readout for point-of-care immunoassay, ACS sensors, 4 (2019) 2272-2276.

[30] R.J. Zeng, J.M. Tao, D.P. Tang, D. Knopp, J. Shu, X. Cao, Biometric-based tactile chemomechanical transduction: An adaptable strategy for portable bioassay, Nano Energy, 71

(2020) 104580.

[31] Y.J. Gao, E.W. Schaler, K. Chen, A. Zhao, W. Gao, H.M. Fahad, Y.G. Leng, A.Z. Zheng, F.R. Xiong, C.C. Zhang, L.C. Tai, P.D. Zhao, R.S. Fearing, A. Javey, Wearable microfluidic diaphragm pressure sensor for health and tactile touch monitoring, Adv. Mater. 29 (2017) 1701985.

[32] S.Z. Lv, Y. Tang, K.Y. Zhang, D.P. Tang, Wet NH_3-triggered NH_2-MIL-125 (Ti) structural switch for visible fluorescence immunoassay impregnated on paper, Anal. Chem. 90 (2018) 14121-14125.

[33] P.H. Zhang, Y. Wang, J. Lian, Q. Shen, C. Wang, B.H. Ma, Y.C. Zhang, T.T. Xu, J.X. Li, Y.P. Shao, F. Xu, J.J. Zhu, Drug Delivery: Engineering the surface of smart nanocarriers using a pH-/thermal-/GSH-responsive polymer zipper for precise tumor targeting therapy in vivo, Adv. Mater. 29 (2017) 1702311.

[34] A. Bagheri, H. Arandiyan, C. Boyer, M. Lim, Lanthanide-doped upconversion nanoparticles: emerging intelligent light-activated drug delivery systems, Adv. Sci. 3 (2016) 1500437.

[35] X.X. Yao, X.X. Niu, K.X. Ma, P. Huang, J.L. Grothe, S. Kaskel, Y.F. Zhu, Graphene quantum dots-capped magnetic mesoporous silica nanoparticles as a multifunctional platform for controlled drug delivery, magnetic hyperthermia, and photothermal therapy, Small, 13 (2017) 1602225.

[36] P. Mostafalu, G. Kiaee, G. Giatsidis, A. Khalilpour, M. Nabavinia, M.R. Dokmeci, S. Sonkusale, D.P. Orgill, A. Tamayol, A. Khademhosseini, A textile dressing for temporal and dosage controlled drug delivery, 27 (2017) 1702399.

[37] P. Mostafalu, A. Tamayol, R. Rahimi, M. Ochoa, A. Khalilpour, G. Kiaee, I.K. Yazdi, S.

Bagherifard, M.R. Dokmeci, B. Ziaie, S.R. Sonkusale, A. Khademhosseini, Smart bandage for monitoring and treatment of chronic wounds, Small, 14 (2018) 1703509.

[38] Z. Ye, H. Tai, R. Guo, Z. Yuan, C. Liu, Y. Su, Z. Chen, Y. Jiang, Excellent ammonia sensing performance of gas sensor based on graphene/titanium dioxide hybrid with improved morphology, Appl. Surf. Sci. 419 (2017) 84–90.

[39] H. Tai, Z. Yuan, W. Zheng, Z. Ye, C. Liu, X. Du, ZnO nanoparticles/reduced graphene oxide bilayer thin films for improved NH_3-sensing Performances at room temperature, Nanoscale Res. Lett. 11 (2016) 130-137.

[40] S. Bai, Y. Zhao, J. Sun, Y. Tian, R. Luo, D. Li, A. Chen, Ultrasensitive room temperature NH_3 sensor based on graphene-polyaniline hybrid loading on PET thin film, Chem. Commun. 51 (2012) 7524-7527.

[41] X. Huang, N. Hu, R. Gao, Y. Yu, Y. Wang, Z. Yang, E. Kong, H. Wei, Y. Zhang, Reduced graphene oxide–polyaniline hybrid: Preparation, characterization and its applications for ammonia gas sensing, J. Mater. Chem. 22 (2012) 22488.

[42] D.C. Tiwari, P. Atri, R. Sharma, Sensitive detection of ammonia by reduced graphene oxide/polypyrrole nanocomposites, Synthetic Met. 203 (2015) 228–234.

[43] X. Tang, D. Lahem, J.-P. Raskin, P. Gerard, X. Geng, N. Andre, M. Debliquy, A fast and room- temperature operation ammonia sensor based on compound of graphene with polypyrrole, IEEE Sens. J. 18 (2018) 9088–9096.

Fig. 1 Schematic of the fabrication of SA/rGO/PPy composite fabric.

Fig. 2 FE-SEM images of pristine SA fabric (a), SA/GO fabric (b), SA/rGO fabric (c) and SA/rGO/PPy fabric (d) with high magnification of PPy nanoparticles in the inserted image. The scale bar is 10 μm.

Fig. 3 (a) Raman spectra of SA fabric, SA/GO fabric, SA/rGO fabric, SA/PPy fabric and SA/rGO/PPy composite fabric, C1s XPS core-level spectra of SA/GO fabric (b) and SA/rGO fabric (c), C1s (d) and N1s (e) XPS core-level spectra of SA/rGO/PPy composite fabric, (f) XRD profile of SA/rGO/PPy composite fabric.

Fig. 4 (a) Stress-strain curve of SA/rGO/PPy composite fabric, (b) TGA analysis of SA/rGO/PPy composite fabric, (c) Rs values of SA/rGO/PPy composite fabric after various laundry cycles.

Fig. 5 (a) The NH_3 gas concentration dependency of R_{rel} sensing response for SA/rGO/PPy composite fabric in the range of 2 to 16 ppm, (b) Log-Log linear fitting curve of sensing response for SA/rGO/PPy composite fabric as a function of NH_3 gas concentration, (c) R_{rel} sensing response to NH_3 gas for SA/rGO/PPy composite fabric versus time undergoing 5 successive cycles at 3 ppm, (d) Selectivity of SA/rGO/PPy sensor with various analytes.

Fig. 6 Time-dependent temperature changes of SA/rGO/PPy composite fabric under different applied voltages (a), Linear fitting curve of temperature of SA/rGO/PPy composite fabric as a function of voltages.

Table 1

Analysis $L_9(3^4)$ orthogonal experimental design of GO thermal-press reduction

No.	GO concentration ($mg \cdot ml^{-1}$)	Temperature (℃)	Time (min)	R_s ($k\Omega \cdot sq^{-1}$)
1	1	160	30	987.64
2	1	180	60	19.70
3	1	200	90	6.87
4	3	160	60	47.40
5	3	180	90	4.38
6	3	200	30	3.39
7	5	160	90	12.00
8	5	180	30	27.47
9	5	200	60	3.14
K1	338.07	349.01	339.5	
K2	18.39	17.18	23.41	
K3	14.20	4.47	7.75	
R	323.87	344.54	331.75	

Table 2

Analysis $L_9(3^4)$ orthogonal experimental design of Py monomer in-situ polymerization

No.	Py concentration ($mol \cdot L^{-1}$)	Ratio of Py and $FeCl_3$	Time (min)	R_s ($k\Omega \cdot sq^{-1}$)
1	0.1	2:1	60	3.48
2	0.1	1:1	120	3.32
3	0.1	1:2	180	2.07
4	0.2	2:1	120	2.40
5	0.2	1:1	180	0.38
6	0.2	1:2	60	1.33
7	0.3	2:1	180	2.17
8	0.3	1:1	60	2.21
9	0.3	1:2	120	0.17
K1	2.96	2.68	2.34	
K2	1.37	1.97	1.96	
K3	1.52	1.19	1.54	
R	1.44	1.49	0.80	

Table 3

Comparisons of NH_3 gas sensing performance among SA/rGO/PPy composite fabric and other reported gas sensing materials

Materials	Low detection limit (ppm)	Sensitivity (%/ppm)	Response time (s)	Recovery time (s)	Ref.
TiO_2/rGO	5	0.2	114	304	38
ZnO/rGO	10	0.1	84	216	39
PANI/rGO	10	3.4	20	27	40
PANI/rGO-MnO_2	5	1.2	1080	240	41
PPy/rGO	3	0.1	147	Heating	42
PPy/G	1	1.7	150	325	43
SA/rGO/PPy	2	5.4	19	24	In this work

1. Reduced graphene oxide (rGO) is prepared by thermal-press reduction.

2. Polypyrrole (PPy) is prepared by in-situ polymerization.

3. SA/rGO/PPy fabric is optimized through L9(3^4) orthogonal experimental design.

4. Multifunctional SA/rGO/PPy fabric can be used as NH_3 gas sensor and heater.

5. SA/rGO/PPy fabric is designed for wearable closed-loop POC application.

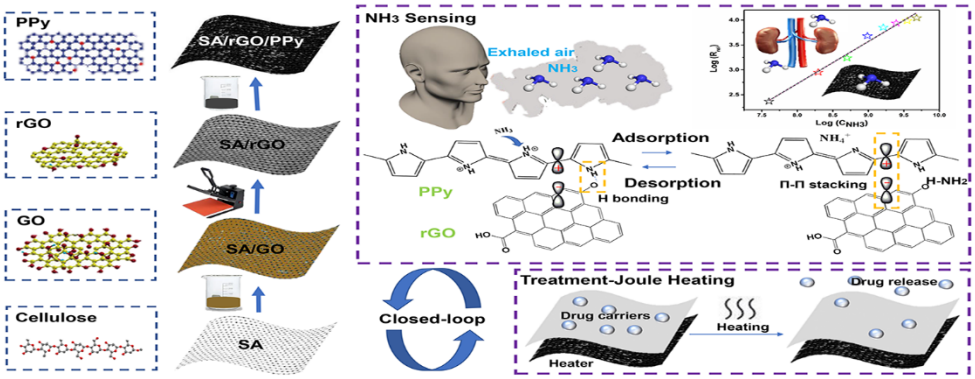

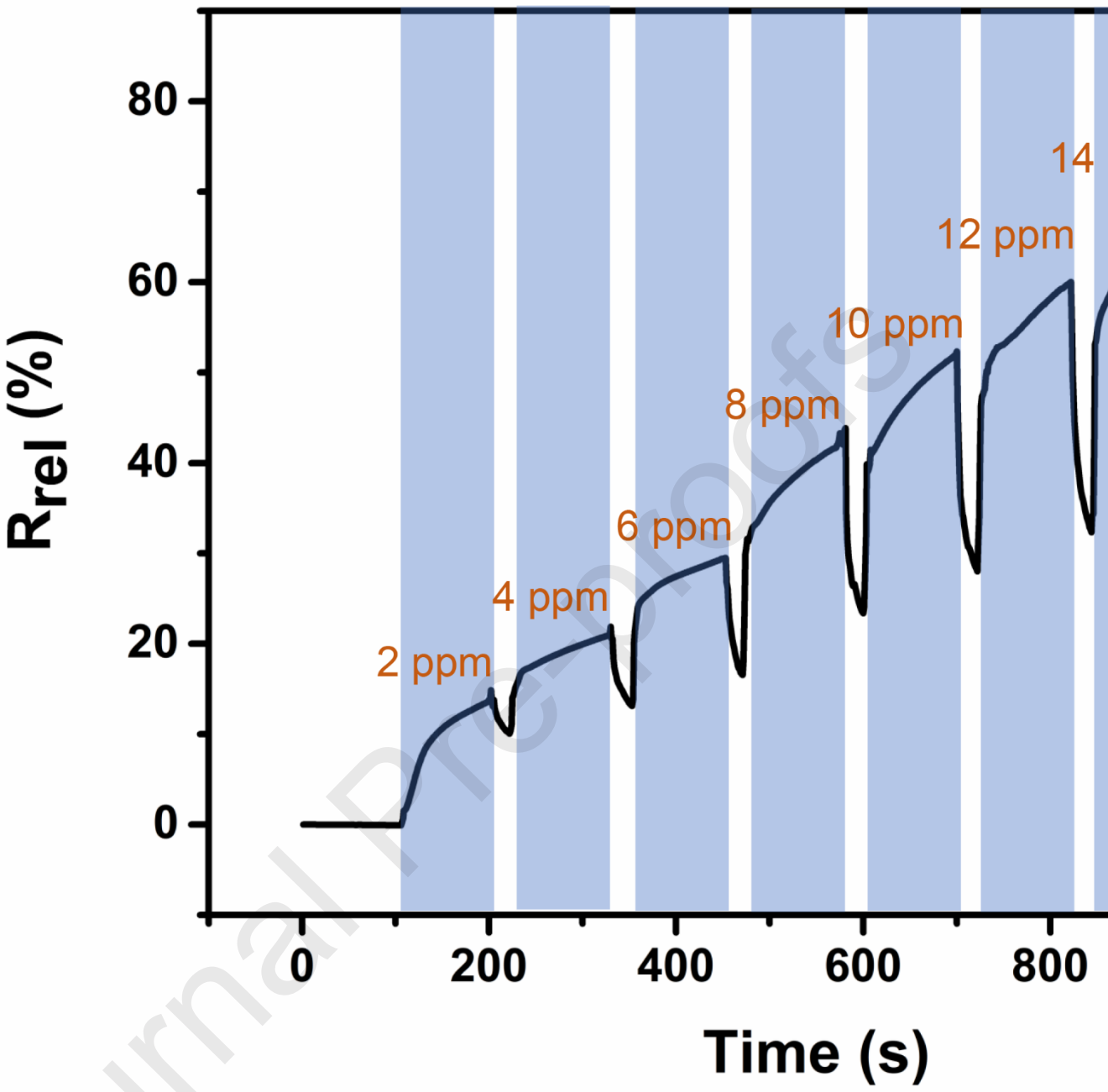

(a)

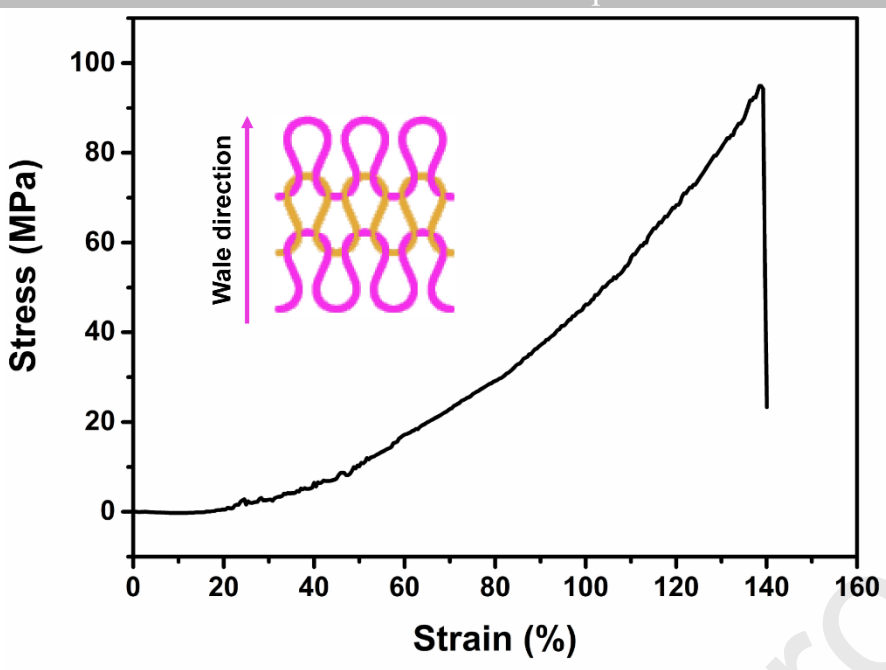

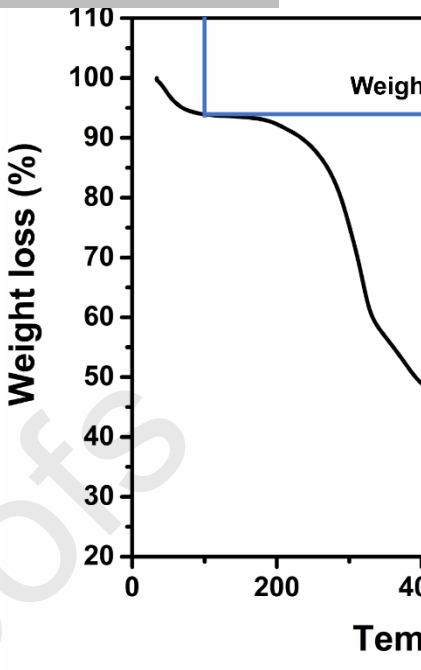

(a)

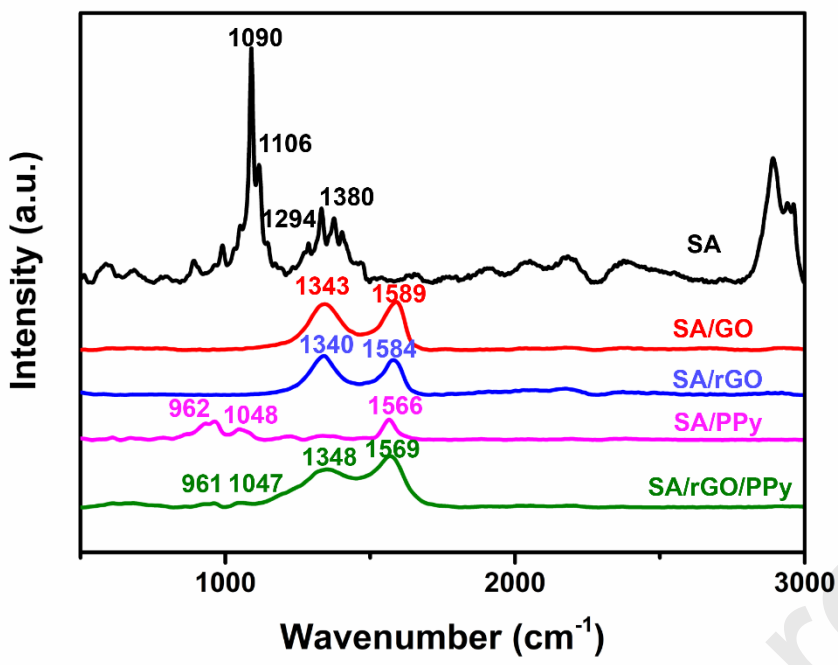

(a)

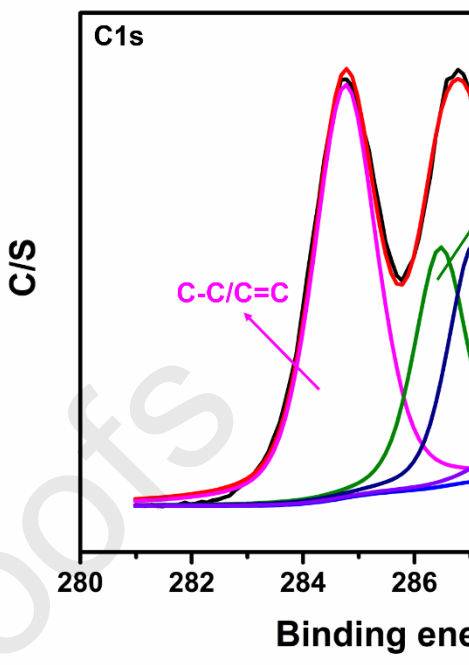

(b)

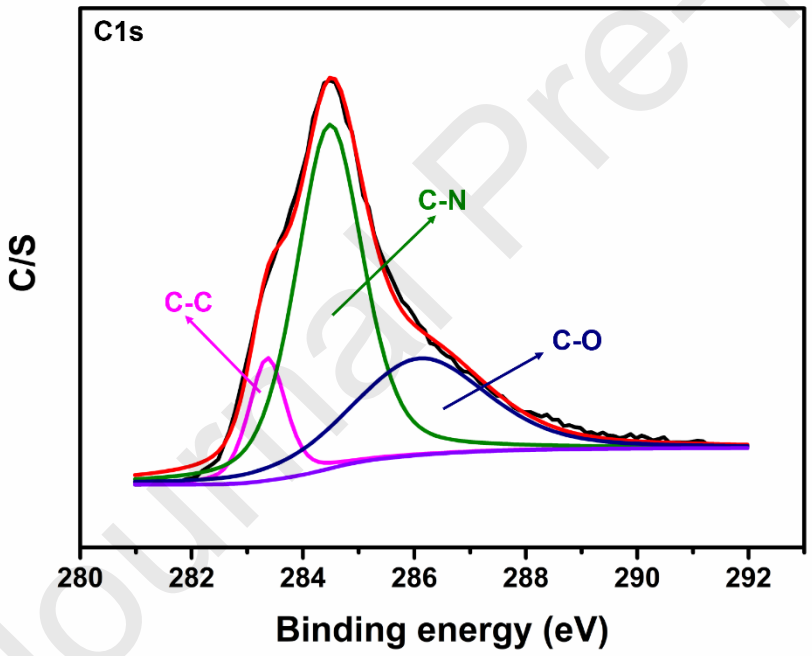

(d)

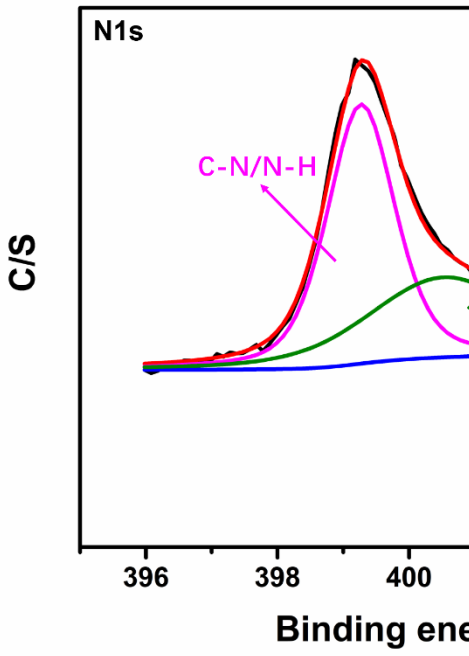

(e)

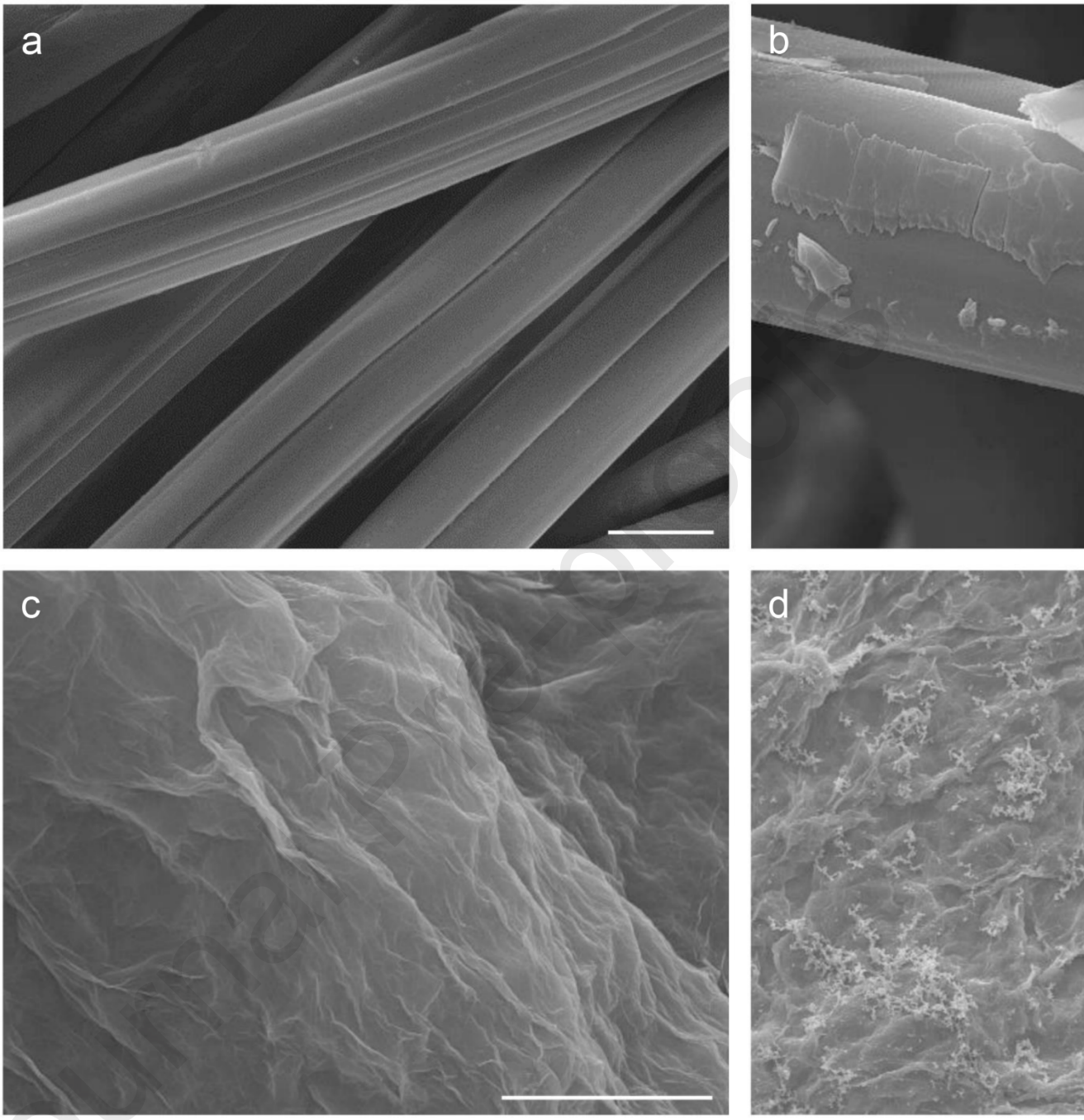

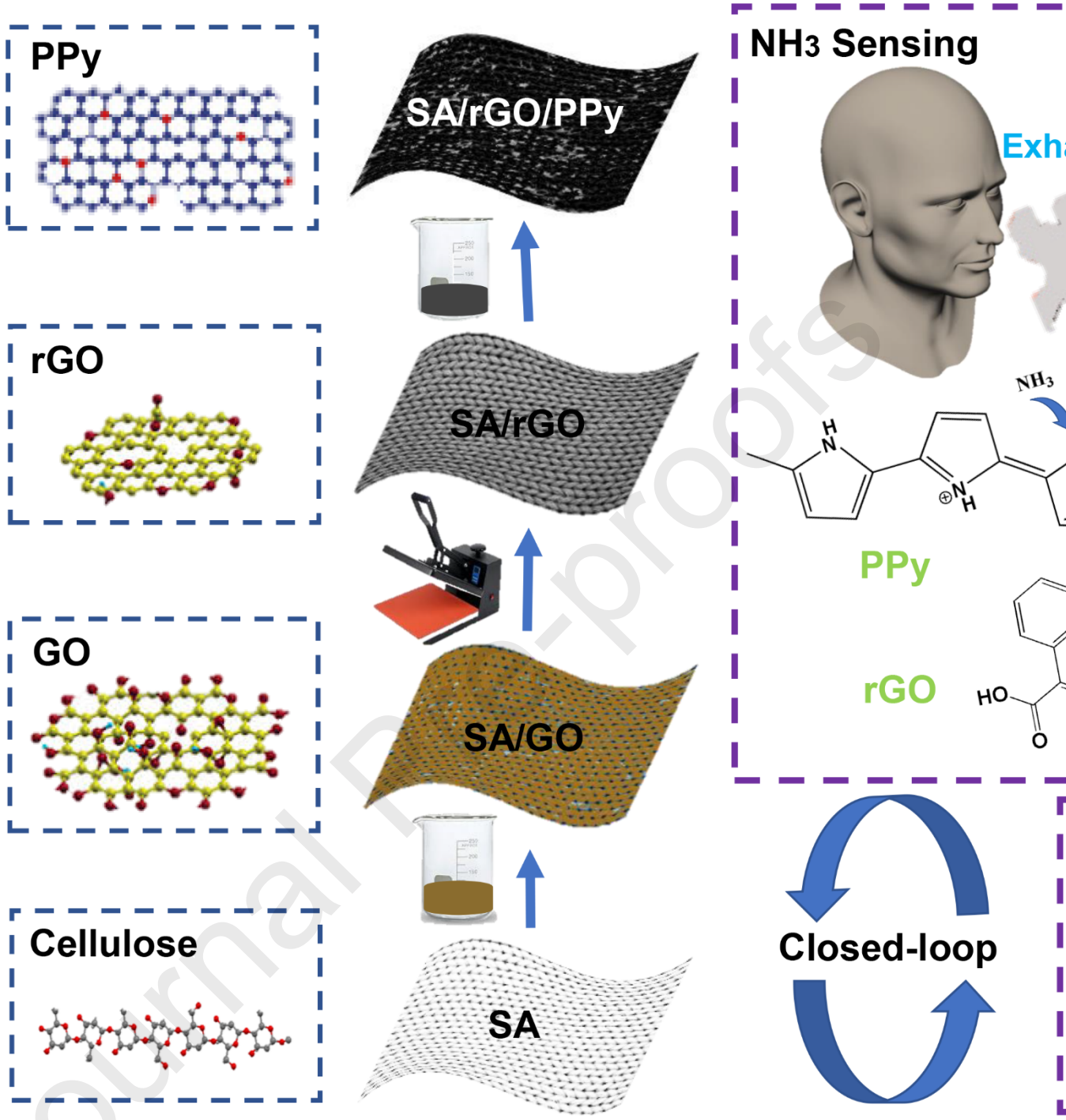

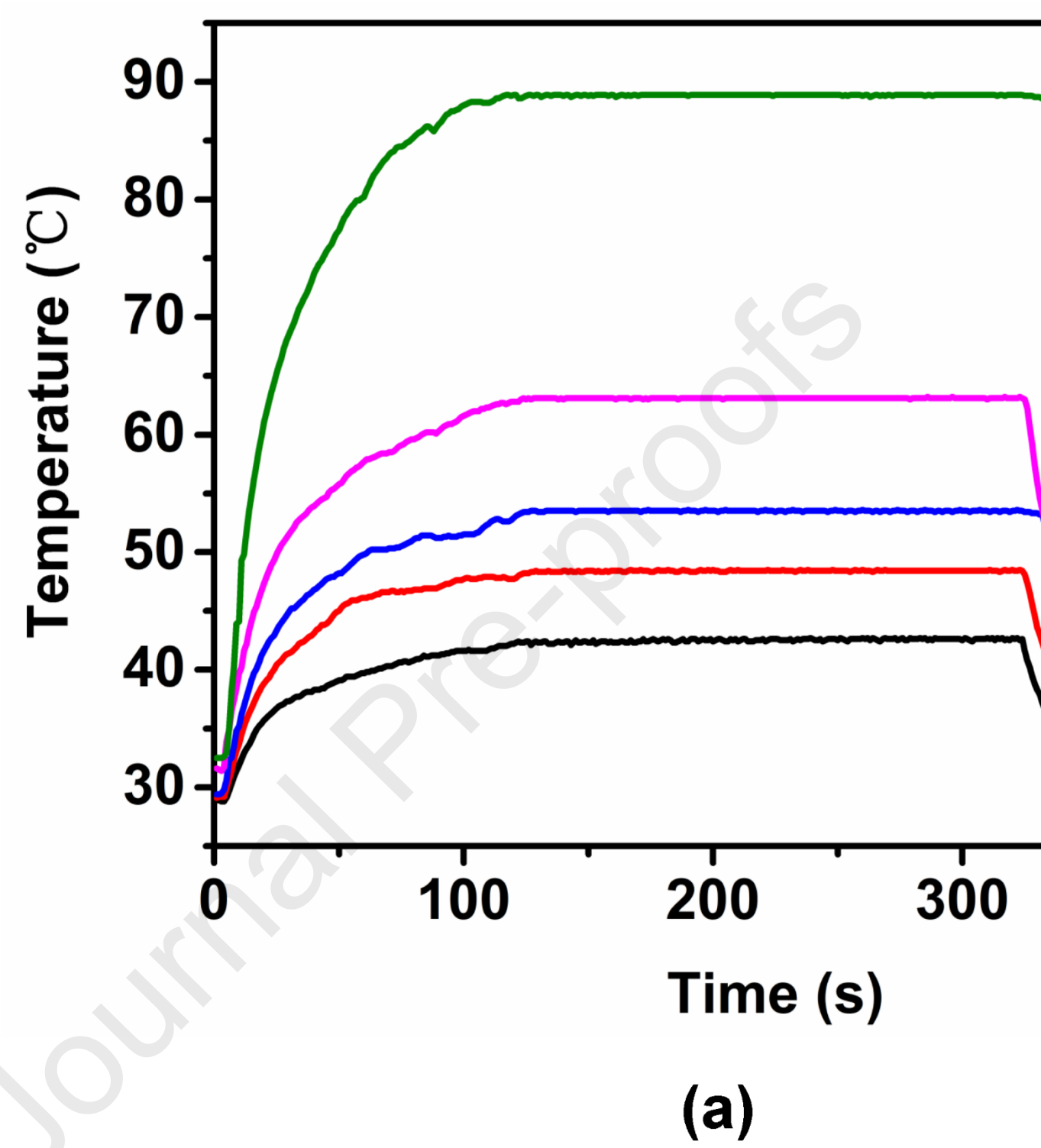

(a)